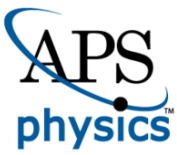

Experimental Measurement of Out-of-Time-Ordered Correlators at Finite Temperature

Alaina M. Green, A. Elben, C. Huerta Alderete, Lata Kh Joshi, Nhung H. Nguyen, Torsten V. Zache, Yingyue Zhu, Bhuvanesh Sundar, and Norbert M. Linke

Phys. Rev. Lett. **128**, 140601 — Published 6 April 2022

DOI: 10.1103/PhysRevLett.128.140601

Experimental measurement of out-of-time-ordered correlators at finite temperature

Alaina M. Green,[1] A. Elben,[2,3,4] C. Huerta Alderete,[1] Lata Kh Joshi,[3,4] Nhung H. Nguyen,[1]
Torsten V. Zache,[3,4] Yingyue Zhu,[1] Bhuvanesh Sundar,[4,5] and Norbert M. Linke[1]

[1] *Joint Quantum Institute and Department of Physics, University of Maryland, College Park, MD 20742, USA*
[2] *Institute for Quantum Information and Matter and Walter Burke Institute for Theoretical Physics, California Institute of Technology, Pasadena, CA 91125, USA*
[3] *Center for Quantum Physics, University of Innsbruck, Innsbruck A-6020, Austria*
[4] *Institute for Quantum Optics and Quantum Information of the Austrian Academy of Sciences, Innsbruck A-6020, Austria*
[5] *JILA, Department of Physics, University of Colorado, Boulder, CO 80309, USA*

(Dated: March 3, 2022)

Out-of-time-ordered correlators (OTOCs) are a key observable in a wide range of interconnected fields including many-body physics, quantum information science, and quantum gravity. Measuring OTOCs using near-term quantum simulators will extend our ability to explore fundamental aspects of these fields and the subtle connections between them. Here, we demonstrate an experimental method to measure OTOCs at finite temperatures and use the method to study their temperature dependence. These measurements are performed on a digital quantum computer running a simulation of the transverse field Ising model. Our flexible method, based on the creation of a thermofield double state, can be extended to other models and enables us to probe the OTOC's temperature-dependent decay rate. Measuring this decay rate opens up the possibility of testing the fundamental temperature-dependent bounds on quantum information scrambling.

INTRODUCTION

A key piece in our understanding of quantum many-body dynamics is the scrambling of quantum information. Out-of-time-ordered correlators (OTOCs) are powerful tools to probe quantum information scrambling in quantum many-body systems. OTOCs are multi-point correlation functions evaluated between operators with the probe times appearing out of order [1]. In particular, the decay of the magnitude of the four-point OTOCs with time indicates the distribution of an initially local perturbation over the system's degrees of freedom, i.e. the scrambling of quantum information. In analogy to chaotic classical systems which are characterized by their sensitivity towards small perturbations, OTOCs were originally recognized in high-energy physics literature [2–4] as probes of quantum chaos. They are now routinely used as tools to study the dynamics of many-body quantum systems [5–11], out-of-equilibrium fluctuations [12–14], quantum phase transitions [15–23], and to elucidate quantum information spreading in black holes through the AdS/CFT correspondence [2–4, 24–28].

It is of fundamental importance to measure OTOCs at finite temperature to study the effects of temperature on information scrambling. The advancement of techniques for measuring thermal OTOCs will serve to experimentally verify the theoretical conjecture on the maximum rate of scrambling [2, 29].

There have recently been several theoretical proposals [30–35] to measure the thermal OTOC, but none have been realized so far. Measuring OTOCs in experiment poses a few stringent requirements, such as the realization of coherent backward time evolution - which is typically required due to the out-of-time ordering of the operators in its definition - and preparation of systems at controllable finite temperature. Previous experiments have measured OTOCs in pure initial states or at infinite temperature in several platforms including NMR [36, 37], superconducting circuits [38, 39], trapped ions [40–42], and cold atoms [43]. While all these experiments relied on the ability to realize backward time evolution, OTOCs have also been measured at infinite temperature using randomized measurements without requiring backward time evolution [42, 44].

In this Letter, we demonstrate the experimental measurement of thermal OTOCs using a digital quantum computer based on trapped ions. Our platform allows individual control of each qubit, and implements a universal gate set that can simulate arbitrary quantum dynamics as Trotterized Hamiltonian evolution [45]. We prepare a thermal state on a subsystem of a larger pure state, constituting a thermofield double state (TFD) [46], using variational quantum circuits as previously demonstrated in Refs. [47, 48]. These capabilities allow us to measure thermal OTOCs in a transverse-field Ising chain of three qubits, based on earlier theoretical proposals [33, 34]. We measure information scrambling by tracking the decay of the magnitude of the thermal OTOC with time. As a key result, we demonstrate that temperature plays a significant role in scrambling, and that information scrambles faster at higher temperatures.

METHODS AND MODEL

Our goal is to measure the following form of the thermal OTOC at inverse temperature $\beta = 1/T$ for a Hamil-

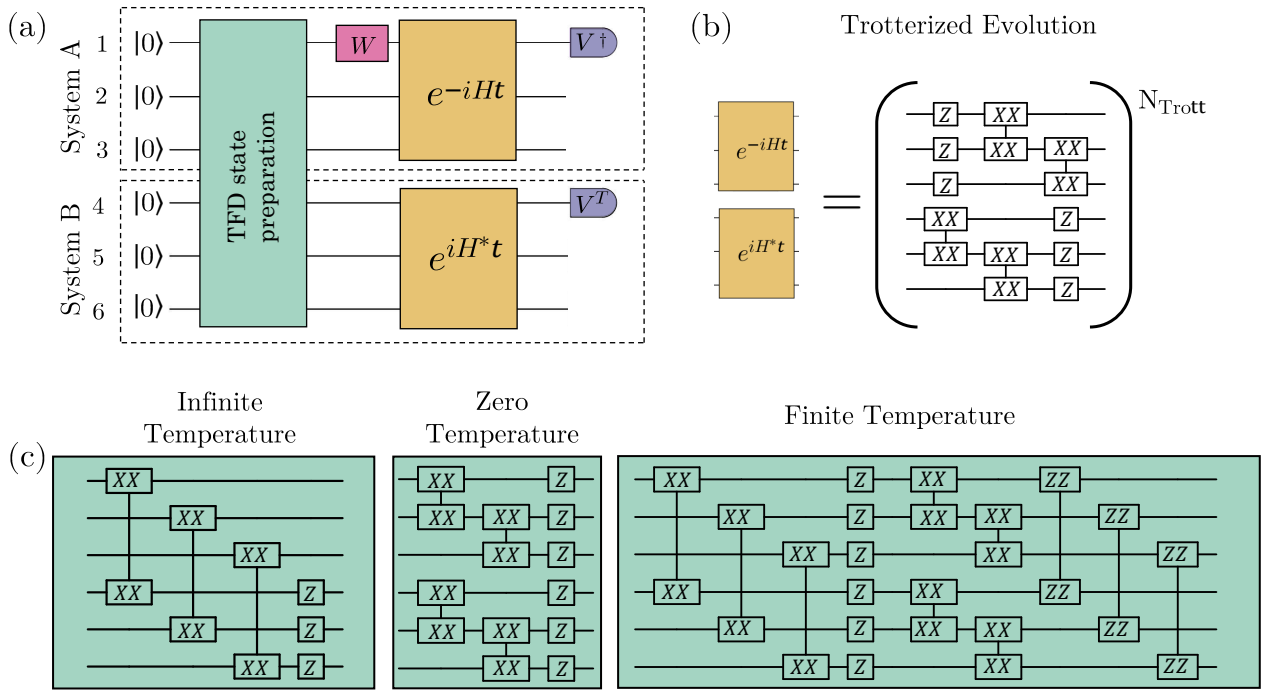

FIG. 1. An overview of the circuit executed on the trapped-ion quantum computer for OTOC measurement at various temperatures in the TFIM. Two copies of the three-spin system are represented by six qubits as shown in (a). From the $|0\rangle^{\otimes N}$ state, the TFD state is prepared using the circuits appropriate for the chosen temperature shown in (c). For the finite temperature TFD state, the set of angles assigned to the gates shown determine the temperature. The perturbing operator $\hat{W}$ imparts local information onto one copy system and each copy is evolved with the appropriate Hamiltonian digitized as shown in (b). Finally, correlations between the two system copies, $\langle \hat{V}^\dagger \otimes \hat{V}^T \rangle$, are measured to determine the OTOC. Here $XX = e^{-i\frac{\theta}{2}\hat{\sigma}_i^x \hat{\sigma}_j^x}$, $ZZ = e^{-i\frac{\theta}{2}\hat{\sigma}_i^z \hat{\sigma}_j^z}$, and $Z = e^{-i\frac{\theta}{2}\hat{\sigma}_i^z}$, where i and j are qubit indices and θ is the rotation angle. The values of θ are given in [49].

tonian $\hat{H}$:

$$O = \frac{1}{Z}\mathrm{Tr}\left(e^{-\beta\hat{H}/2}\hat{W}^\dagger\hat{V}^\dagger(t)\hat{W}e^{-\beta\hat{H}/2}\hat{V}(t)\right), \quad (1)$$

where $\hat{V}(t) = e^{i\hat{H}t}\hat{V}e^{-i\hat{H}t}$ is Hermitian and $\hat{W}$ is a local unitary operator. The normalization factor is given by $Z = \mathrm{Tr}[e^{-\beta\hat{H}}]$. We take $\hbar = k_B = 1$.

The experimental sequence for measuring O, based on previous theoretical proposals [33, 34], is summarized in Fig. 1(a). Central to our method is the creation of a TFD state spanning two system copies labelled A and B, each of N-qubits, and taking the form

$$|\psi_{\mathrm{TFD}}\rangle = \frac{1}{\sqrt{Z}}\sum_n e^{-\beta E_n/2}|n\rangle_A|n^*\rangle_B, \quad (2)$$

where n labels the eigenstates of $\hat{H}$ in each copy with energies E_n, and the star indicates the complex conjugate state. Although $|\psi_{\mathrm{TFD}}\rangle$ is a pure state, expectation values taken with respect to the TFD state give thermally averaged results for each system copy. Denoting the Hamiltonian for each system copy as $\hat{H}_A$ and $\hat{H}_B$, and the initial perturbation as $\hat{W}$, we first apply $\hat{W}_A$ on copy A in the initial state, and then evolve the two-copy system with $\hat{H}_A - \hat{H}_B^*$ as shown in Fig. 1(a). The state just after time evolution is given by:

$$|\psi(t)\rangle = e^{-i(\hat{H}_A - \hat{H}_B^*)t}\hat{W}_A|\psi_{\mathrm{TFD}}\rangle. \quad (3)$$

Operators $\hat{V}_A$ and $\hat{V}_B$ are mirrored between the two copies and constitute the local measurements giving access to the OTOC in the form of their correlator:

$$\langle\psi(t)|\hat{V}_A^\dagger \otimes \hat{V}_B^T|\psi(t)\rangle = \frac{1}{Z}\sum_{n,m}\langle m|_A\langle m^*|_B e^{-\beta E_m/2}\hat{W}_A^\dagger e^{i(\hat{H}_A - \hat{H}_B^*)t}\hat{V}_A^\dagger \otimes \hat{V}_B^T e^{-i(\hat{H}_A - \hat{H}_B^*)t}e^{-\beta E_n/2}\hat{W}_A|n\rangle_A|n^*\rangle_B. \quad (4)$$

We split the expectation value in the joint Hilbert space of A and B in Eq. (4) into a product of two matrix elements separately in the A and B Hilbert spaces, and hereafter drop the labels. We obtain

$$\langle\psi(t)|\,\hat{V}^\dagger\otimes\hat{V}^T\,|\psi(t)\rangle = \frac{1}{Z}\sum_{n,m}\langle m^*|e^{-i\hat{H}^*t}\hat{V}^T e^{i\hat{H}^*t}|n^*\rangle \times\langle m|e^{-\beta E_m/2}\hat{W}^\dagger e^{i\hat{H}t}\hat{V}^\dagger e^{-i\hat{H}t}e^{-\beta E_n/2}\hat{W}|n\rangle\,. \tag{5}$$

Subsequently, we utilize the relations $e^{-\beta E_n/2}\,|n\rangle = e^{-\beta\hat{H}/2}\,|n\rangle$ and $\langle m^*|\,e^{-i\hat{H}^*t}\hat{V}^T e^{i\hat{H}^*t}\,|n^*\rangle = \langle n|\,\hat{V}(t)\,|m\rangle$ to obtain:

$$\langle\psi(t)|\,\hat{V}^\dagger\otimes\hat{V}^T\,|\psi(t)\rangle = \frac{1}{Z}\sum_{n,m}\langle m|\,e^{-\beta\hat{H}/2}\hat{W}^\dagger\hat{V}^\dagger(t)\hat{W}e^{-\beta\hat{H}/2}\,|n\rangle\,\langle n|\,\hat{V}(t)\,|m\rangle\,. \tag{6}$$

Resolving the identity operator in Eq. (6) [50], $\sum_n|n\rangle\langle n| = \hat{1}$, we find that the right hand side of Eq. (6) reduces to O in Eq. (1).

To demonstrate our method, we choose to study OTOCs in the transverse-field Ising model (TFIM), which can be very efficiently simulated on a trapped-ion quantum computer (TIQC). The Hamiltonian for this model is:

$$\hat{H} = J\sum_{i=1}^{N-1}\hat{\sigma}_i^x\hat{\sigma}_{i+1}^x + g\sum_{i=1}^{N}\hat{\sigma}_i^z, \tag{7}$$

where J gives the spin-spin coupling strength, g determines the strength of the interaction with the field, and $\hat{\sigma}_i^\alpha$, $\alpha\in(x,y,z)$ are Pauli spin operators on the ith site. Note that $\hat{H}^* = \hat{H}$. Time evolution is performed through Trotterization, in which the full evolution is approximated by executing one Trotter step sequentially N_{Trott} times. The digital circuit for each Trotter step is represented in brackets in Fig. 1(b). It is constructed from single-qubit rotations and two-qubit entangling gates. The parameters for these gates, i.e. their angles of rotation on the single or two-qubit Bloch sphere, determine the evolution time spanned by a single Trotter step.

In order to prepare the TFD state, we follow the variational method in Refs. [47, 48] with classically optimized parameters. This method digitally approximates the true thermal state. We use classical simulation of the quantum circuit to quantify this approximation and find that, in the absence of physical errors, this method would allow us to create TFD states with fidelity greater than 97% for all temperatures considered in this work. However, physical errors limit the fidelity of our experimentally prepared state to less than 97%. Note that in the case of infinite temperature, the theoretical preparation circuit requires no approximation. For the finite temperature preparation circuits, the exact parameters used for the gates determine the temperature of the OTOC measurement.

We execute these circuits on a TIQC, which has previously been described in Ref. [51]. The TIQC is built upon a trapped linear chain of $^{171}Yb^+$ ions with the qubit encoded in two different hyperfine ground states. All qubits are initialized in the $|0\rangle$ state via optical pumping [52]. Coherent operations are implemented using a pair of Raman beams derived from a mode-locked laser at 355 nm. The beams are counter-propagating and one of them is split into an array of tightly focused beams, each addressing a single ion in the chain. Single-qubit gates are compiled into pulses of appropriate phase, amplitude and duration to effect a resonant Rabi rotation while two-qubit gates are compiled into amplitude and frequency modulated pulses which effectively entangle the qubits' spin degrees of freedom through transient entanglement of both spins with the shared motion of the ions in the Paul trap [53, 54]. The typical fidelities of single- and two-qubit gates are 99.5% and 98.5%, respectively. Measurements are performed in the computational basis with state-dependent fluorescence detection [52]. The entire experiment is repeated several thousand times to detect the average state population, which is corrected for errors of about 1% arising from imperfect state preparation and measurement that are independently characterized.

RESULTS

We measure the OTOCs in the TFIM at different times, set by our Trotter steps, by executing the circuits in Fig. 1. Fig. 2 shows time evolution of the OTOC for two different temperatures. In this case we choose $\hat{W} = \hat{\sigma}_1^x$ and we measure the correlator $\langle\hat{V}^\dagger\otimes\hat{V}^T\rangle = \langle\hat{\sigma}_1^z\otimes\hat{\sigma}_4^z\rangle$, although any corresponding pair between the two copies of the system could be used. We compare the experimentally measured results to those of the expected results which can be calculated exactly in this small demonstration. The observed decay of the OTOC's magnitude from its initial temperature-dependent value agrees well with the expected result. The deviation between the measured results (pink circles) and the exact evolution (purple line) can be attributed to two general errors: those arising from algorithmic approximations and those arising from physical errors on the apparatus. Algorithmic errors comprise both imperfect variational preparation of the TFD state and Trotter error, and can be read in Fig. 2 as the difference between the purple line and the green triangles. As can be seen in the Fig. 2, algorithmic error is small compared to the physical error which is likely dominated by imperfect calibration of the gates or residual entanglement of the qubit states with the ion motion.

A small portion of the physical error can be eliminated through post selection whereby we take advantage of the symmetry of our model to discard results which could only arise through physical error. The sym-

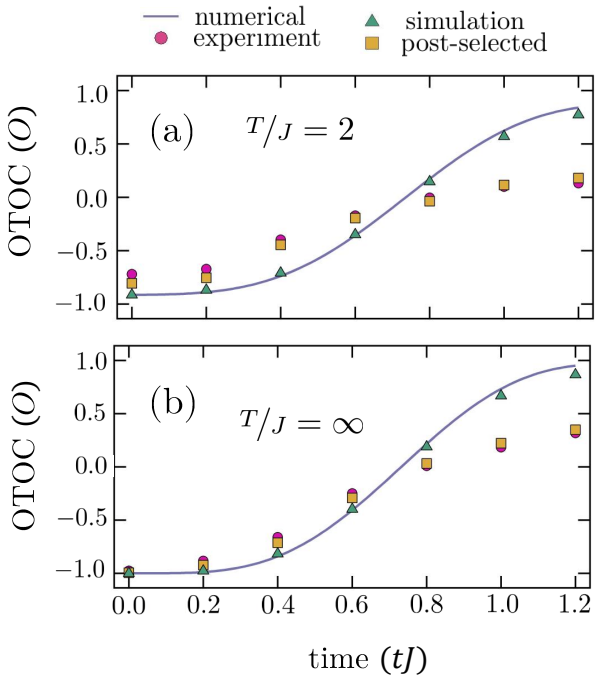

FIG. 2. The evolution of the OTOC is measured as summarized in Fig. 1. Here we have prepared the TFD state for $T/J = 2$ in (a) $T/J = \infty$ in (b) and chosen $J = g$ (see Eq. (7)). In both cases we use $\langle \hat{V}^\dagger \otimes \hat{V}^T \rangle = \langle \hat{\sigma}_1^z \otimes \hat{\sigma}_4^z \rangle$ for our measurement and have used $\hat{W} = \hat{\sigma}_1^x$ to impart local information. Pink circles show the experimental result, yellow squares the experimental result after post-selection (see text), green triangles the expected results in an error-free circuit, and the purple line corresponds to numerical simulation of the model. For the experimental values, the statistical error bars are smaller than the symbols. While the two OTOCs at both temperatures exhibit qualitatively similar decay, close inspection shows a significant difference in the rate of decay (see Fig. 3).

metry of the TFIM dictates that its eigenstates satisfy $\prod_{i=1}^{2N} \hat{\sigma}_i^z |n\rangle |n^*\rangle = |n\rangle |n^*\rangle$, and we therefore have $\langle \psi_{\text{TFD}} | \prod_{i=1}^{2N} \hat{\sigma}_i^z | \psi_{\text{TFD}} \rangle = 1$ and $\langle \psi_{\text{TFD}} | \hat{\sigma}_1^x \left(\prod_{i=1}^{2N} \hat{\sigma}_i^z \right) \hat{\sigma}_1^x | \psi_{\text{TFD}} \rangle = -1$. Noting that the initial state before time evolution is $|\psi(0)\rangle = \hat{\sigma}_1^x |\psi_{\text{TFD}}\rangle$, and because $\prod_{i=1}^{2N} \hat{\sigma}_i^z$ commutes with $\hat{H}_A - \hat{H}_B^*$, any experimental results for which $\langle \prod_{i=1}^{2N} \hat{\sigma}_i^z \rangle \neq -1$ may be discarded. For the entirety of the results shown in Figures 2(a) and (b) respectively, an average of 40% and 20% of the measurements are discarded in post selection. While the value of $\langle \hat{V}^\dagger \otimes \hat{V}^T \rangle$ grows from an initial value near -1, i.e. its magnitude decays, as expected by the numerical simulation, the decay is damped through physical errors. Separating further physical errors from genuine decay of the OTOC will be treated heuristically below.

As our main result, we show the dependence of the OTOC decay rate with temperature. In order to quantify this, we approximate the derivative, $O'(t)$, by the finite difference λ at the point where the decay of the OTOC is expected to be largest. In particular, we extract $\lambda \equiv \frac{O(0.8/J) - O(0.4/J)}{0.4/J}$. A fair comparison of the OTOC magnitudes' decay at different temperatures requires a similar amount of physical error in all the circuits. To accomplish this, we artificially add gates to the shorter depth circuits such that the number of gates are the same for a given time. In particular, we add to state preparation extra gates which do not affect the resulting state except through physical error.

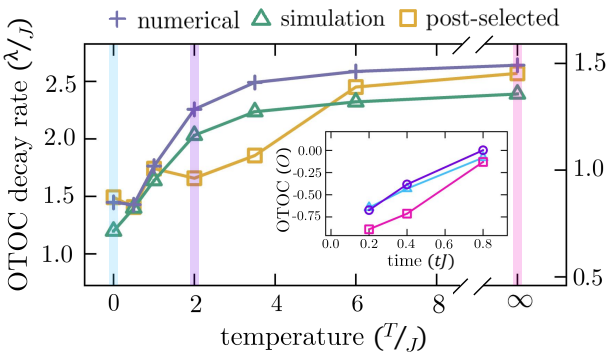

FIG. 3. Temperature-dependence of the OTOC decay rate O', approximated by the finite difference λ (see main text). On the right axis, yellow squares show the experimental results after post selection (see text). On the left axis, green triangles show simulation of the circuit on an error-free quantum computer and the purple plus signs show the slope for the numerical simulation. (inset) Sample evolution of $\langle \hat{V}^\dagger \otimes \hat{V}^T \rangle$ at zero temperature (light blue triangles), for $T/J = 2$ (purple circles) and infinite temperature (pink squares), showing decay of the OTOC magnitude. The Trotter step size is not uniform but proceeds in sizes $\{0.2, 0.2, 0.4\}$ tJ. For the experimental data the statistical error bars are smaller than the symbols.

Fig. 3 shows the OTOC decay rate versus temperature, with the inset showing the magnitude's decay versus time at a few sample temperatures. As expected from the sample results in Fig. 2, the experimentally measured decay rate is lower than the theoretically expected result. In order to better compare the change in decay rate with temperature to theoretical expectations, we choose to plot the experimental decay rate on a different axis than the theoretical ones. The OTOC decay rate is experimentally observed to increase with temperature with a trend similar to that seen in the numerical results.

OUTLOOK

Our measurement of the temperature dependence of OTOC decay represents a new tool for digital quantum simulation, providing a measurable quantity which can be used to study the temperature dependence of quan-

tum information scrambling. In particular, experimental access to thermal OTOCs provides a tantalizing route to using quantum simulators to test fast scrambling and bounds on the rate of information scrambling [2, 29]. This includes testing the exponential decay of OTOCs in fast-scrambling quantum models [55–57], and saturation of the bound in models that are analogous to black holes via holographic duality [24, 25]. Additional building blocks for realizing such a model have already been considered in Refs. [58–60]. Measuring thermal OTOCs also provides a route to implement and benchmark ideas for simulating many-body teleportation and traversable wormholes in the lab [10, 61, 62].

ACKNOWLEDGEMENTS

A.E. acknowledges funding by the German National Academy of Sciences Leopoldina under the grant number LPDS 2021-02 and by the Walter Burke Institute for Theoretical Physics, Caltech. L.K.J. acknowledges the European Union's Horizon 2020 research and innovation programme under Grant Agreement No. 731473 (QuantERA via QT-FLAG) and the Austrian Science Foundation (FWF, P 32597 N). T.V.Z.'s work is supported by the Simons Collaboration on Ultra-Quantum Matter, which is a grant from the Simons Foundation (651440, P.Z.). This work received support from the National Science Foundation through the Quantum Leap Challenge Institute for Robust Quantum Simulation (OMA-2120757) and the Physics Frontier Center (PHY-1430094) at the Joint Quantum Institute (JQI). A.M.G. is supported by a JQI Postdoctoral Fellowship. N.M.L. acknowledges funding by the Maryland-Army-Research-Lab Quantum Partnership (W911NF1920181), the Department of Energy, Office of Science, Office of Nuclear Physics (DE-SC0021143), and the Office of Naval Research (N00014-20-1-2695). We thank Ana Maria Rey and Murray Holland for a careful reading of the manuscript.

[1] B. Swingle, Unscrambling the physics of out-of-time-order correlators, Nature Physics **14**, 988 (2018).
[2] J. Maldacena, S. H. Shenker, and D. Stanford, A bound on chaos, J. High Energy Phys. **2016** (8), 106.
[3] S. H. Shenker and D. Stanford, Black holes and the butterfly effect, J. High Energy Phys. **2014** (3), 67.
[4] S. H. Shenker and D. Stanford, Multiple shocks, J. High Energy Phys. **2014** (12), 46.
[5] R. Fan, P. Zhang, H. Shen, and H. Zhai, Out-of-time-order correlation for many-body localization, Science Bulletin **62**, 707 (2017).
[6] X. Chen, T. Zhou, D. A. Huse, and E. Fradkin, Out-of-time-order correlations in many-body localized and thermal phases, Ann. Phy. **529**, 1600332 (2017).
[7] B. Swingle and D. Chowdhury, Slow scrambling in disordered quantum systems, Phys. Rev. B **95**, 060201(R) (2017).
[8] R.-Q. He and Z.-Y. Lu, Characterizing many-body localization by out-of-time-ordered correlation, Phys. Rev. B **95**, 054201 (2017).
[9] A. Bohrdt, C. B. Mendl, M. Endres, and M. Knap, Scrambling and thermalization in a diffusive quantum many-body system, New J. Phys. **19**, 063001 (2017).
[10] T. Schuster, B. Kobrin, P. Gao, I. Cong, E. T. Khabiboulline, N. M. Linke, M. D. Lukin, C. Monroe, B. Yoshida, and N. Y. Yao, Many-body quantum teleportation via operator spreading in the traversable wormhole protocol (2021), arXiv:2102.00010 [quant-ph].
[11] Y. Huang, Y.-L. Zhang, and X. Chen, Out-of-time-ordered correlators in many-body localized systems, Annalen der Physik **529**, 1600318 (2017).
[12] M. Campisi and J. Goold, Thermodynamics of quantum information scrambling, Phys. Rev. E **95**, 062127 (2017).
[13] N. Yunger Halpern, Jarzynski-like equality for the out-of-time-ordered correlator, Phys. Rev. A **95**, 012120 (2017).
[14] N. Yunger Halpern, B. Swingle, and J. Dressel, Quasiprobability behind the out-of-time-ordered correlator, Phys. Rev. A **97**, 042105 (2018).
[15] R. J. Lewis-Swan, S. R. Muleady, and A. M. Rey, Detecting out-of-time-order correlations via quasiadiabatic echoes as a tool to reveal quantum coherence in equilibrium quantum phase transitions, Phys. Rev. Lett. **125**, 240605 (2020).
[16] X. Nie, B.-B. Wei, X. Chen, Z. Zhang, X. Zhao, C. Qiu, Y. Tian, Y. Ji, T. Xin, D. Lu, and J. Li, Experimental observation of equilibrium and dynamical quantum phase transitions via out-of-time-ordered correlators, Phys. Rev. Lett. **124**, 250601 (2020).
[17] C. B. Dağ, K. Sun, and L.-M. Duan, Detection of quantum phases via out-of-time-order correlators, Phys. Rev. Lett. **123**, 140602 (2019).
[18] C. B. Dağ, L.-M. Duan, and K. Sun, Topologically induced prescrambling and dynamical detection of topological phase transitions at infinite temperature, Phys. Rev. B **101**, 104415 (2020).
[19] B.-B. Wei, G. Sun, and M.-J. Hwang, Dynamical scaling laws of out-of-time-ordered correlators, Phys. Rev. B **100**, 195107 (2019).
[20] Z.-H. Sun, J.-Q. Cai, Q.-C. Tang, Y. Hu, and H. Fan, Out-of-time-order correlators and quantum phase transitions in the Rabi and Dicke models, Ann. Phys. (Leipzig) **532**, 1900270 (2020).
[21] Q. Wang and F. Pérez-Bernal, Probing an excited-state quantum phase transition in a quantum many-body system via an out-of-time-order correlator, Phys. Rev. A **100**, 062113 (2019).
[22] M. Heyl, F. Pollmann, and B. Dóra, Detecting equilibrium and dynamical quantum phase transitions in Ising chains via out-of-time-ordered correlators, Phys. Rev. Lett. **121**, 016801 (2018).
[23] H. Shen, P. Zhang, R. Fan, and H. Zhai, Out-of-time-order correlation at a quantum phase transition, Phys. Rev. B **96**, 054503 (2017).
[24] J. Maldacena, The large-n limit of superconformal field theories and supergravity, Int. J. Theor. Phys. **38**, 1113 (1999).
[25] J. Maldacena and D. Stanford, Remarks on the Sachdev-Ye-Kitaev model, Phys. Rev. D **94**, 106002 (2016).

[26] J. Maldacena, D. Standford, and Z. Yang, Diving into traversable wormholes, Fortschritte der Physik **65**, 1700034 (2017).

[27] J. Maldacena and X.-L. Qi, Eternal traversable wormhole (2018), arXiv:1804.00491 [hep-th].

[28] A. Bhattacharyya, L. K. Joshi, and B. Sundar, Quantum information scrambling: From holography to quantum simulators, arXiv preprint arXiv:2111.11945 (2021).

[29] C. Murthy and M. Srednicki, Bounds on chaos from the eigenstate thermalization hypothesis, Phys. Rev. Lett. **123**, 230606 (2019).

[30] N. Y. Yao, F. Grusdt, B. Swingle, M. D. Lukin, D. M. Stamper-Kurn, J. E. Moore, and E. A. Demler, Interferometric approach to probing fast scrambling (2016), arXiv:1607.01801 [quant-ph].

[31] B. Vermersch, A. Elben, L. M. Sieberer, N. Y. Yao, and P. Zoller, Probing scrambling using statistical correlations between randomized measurements, Phys. Rev. X **9**, 021061 (2019).

[32] B. Yoshida and N. Y. Yao, Disentangling scrambling and decoherence via quantum teleportation, Phys. Rev. X **9**, 011006 (2019).

[33] E. Lantagne-Hurtubise, S. Plugge, O. Can, and M. Franz, Diagnosing quantum chaos in many-body systems using entanglement as a resource, Phys. Rev. Research **2**, 013254 (2020).

[34] B. Sundar, A. Elben, L. K. Joshi, and T. V. Zache, Proposal for measuring out-of-time-ordered correlators at finite temperature with coupled spin chains (2021), arXiv:2107.02196 [quant-ph].

[35] J. Dressel, J. R. González Alonso, M. Waegell, and N. Yunger Halpern, Strengthening weak measurements of qubit out-of-time-order correlators, Physical Review A **98**, 012132 (2018).

[36] J. Li, R. Fan, H. Wang, B. Ye, B. Zeng, H. Zhai, X. Peng, and J. Du, Measuring out-of-time-order correlators on a nuclear magnetic resonance quantum simulator, Phys. Rev. X **7**, 031011 (2017).

[37] K. X. Wei, C. Ramanathan, and P. Cappellaro, Exploring localization in nuclear spin chains, Phys. Rev. Lett. **120**, 070501 (2018).

[38] B. Foxen, C. Neill, A. Dunsworth, P. Roushan, B. Chiaro, A. Megrant, J. Kelly, Z. Chen, K. Satzinger, R. Barends, F. Arute, K. Arya, R. Babbush, D. Bacon, J. C. Bardin, S. Boixo, D. Buell, B. Burkett, Y. Chen, R. Collins, E. Farhi, A. Fowler, C. Gidney, M. Giustina, R. Graff, M. Harrigan, T. Huang, S. V. Isakov, E. Jeffrey, Z. Jiang, D. Kafri, K. Kechedzhi, P. Klimov, A. Korotkov, F. Kostritsa, D. Landhuis, E. Lucero, J. McClean, M. McEwen, X. Mi, M. Mohseni, J. Y. Mutus, O. Naaman, M. Neeley, M. Niu, A. Petukhov, C. Quintana, N. Rubin, D. Sank, V. Smelyanskiy, A. Vainsencher, T. C. White, Z. Yao, P. Yeh, A. Zalcman, H. Neven, and J. M. Martinis (Google AI Quantum), Demonstrating a continuous set of two-qubit gates for near-term quantum algorithms, Phys. Rev. Lett. **125**, 120504 (2020).

[39] J. Braumüller, A. H. Karamlou, Y. Yanay, B. Kannan, D. Kim, M. Kjaergaard, A. Melville, B. M. Niedzielski, Y. Sung, A. Vepsäläinen, R. Winik, J. L. Yoder, T. P. Orlando, S. Gustavsson, C. Tahan, and W. D. Oliver, Probing quantum information propagation with out-of-time-ordered correlators (2021), arXiv:2102.11751 [quant-ph].

[40] M. Gärttner, J. G. Bohnet, A. Safavi-Naini, M. L. Wall, J. J. Bollinger, and A. M. Rey, Measuring out-of-time-order correlations and multiple quantum spectra in a trapped-ion quantum magnet, Nature Physics **13**, 781 (2017).

[41] K. A. Landsman, C. Figgatt, T. Schuster, N. M. Linke, B. Yoshida, N. Y. Yao, and C. Monroe, Verified quantum information scrambling, Nature **567**, 61 (2019).

[42] M. K. Joshi, A. Elben, B. Vermersch, T. Brydges, C. Maier, P. Zoller, R. Blatt, and C. F. Roos, Quantum information scrambling in a trapped-ion quantum simulator with tunable range interactions, Phys. Rev. Lett. **124**, 240505 (2020).

[43] S. Pegahan, I. Arakelyan, and J. E. Thomas, Energy-resolved information scrambling in energy-space lattices, Phys. Rev. Lett. **126**, 070601 (2021).

[44] X. Nie, Z. Zhang, X. Zhao, T. Xin, D. Lu, and J. Li, Detecting scrambling via statistical correlations between randomized measurements on an nmr quantum simulator (2019), arXiv:1903.12237 [quant-ph].

[45] D. Zhu, S. Johri, N. H. Nguyen, C. Huerta Alderete, K. A. Landsman, N. M. Linke, C. Monroe, and A. Y. Matsuura, Probing many-body localization on a noisy quantum computer, Phys. Rev. A **103**, 032606 (2021).

[46] Y. Takahashi and H. Umezawa, Thermo field dynamics, Int. J. Mod. Phys. B **10**, 1755 (1996), https://doi.org/10.1142/S0217979296000817.

[47] J. Wu and T. H. Hsieh, Variational thermal quantum simulation via thermofield double states, Phys. Rev. Lett. **123**, 220502 (2019).

[48] D. Zhu, S. Johri, N. M. Linke, K. A. Landsman, C. Huerta Alderete, N. H. Nguyen, A. Y. Matsuura, T. H. Hsieh, and C. Monroe, Generation of thermofield double states and critical ground states with a quantum computer, Proceedings of the National Academy of Sciences **117**, 25402 (2020), https://www.pnas.org/content/117/41/25402.full.pdf.

[49] Supplemental material.

[50] After dropping the unnecessary labels A and B, it is irrelevant that $|n\rangle_A$ and $|n^*\rangle_B$ came from different subsystems. Therefore, the term $\sum_n |n\rangle\langle n|$ is equal to the identity operator.

[51] S. Debnath, N. M. Linke, C. Figgatt, K. A. Landsman, K. Wright, and C. Monroe, Demonstration of a small programmable quantum computer with atomic qubits, Nature **536**, 63 (2016).

[52] S. Olmschenk, K. C. Younge, D. L. Moehring, D. N. Matsukevich, P. Maunz, and C. Monroe, Manipulation and detection of a trapped Yb^+ hyperfine qubit, Phys. Rev. A **76**, 052314 (2007).

[53] K. Mølmer and A. Sørensen, Multiparticle entanglement of hot trapped ions, Phys. Rev. Lett. **82**, 1835 (1999).

[54] R. Blümel, N. Grzesiak, N. H. Nguyen, A. M. Green, M. Li, A. Maksymov, N. M. Linke, and Y. Nam, Efficient stabilized two-qubit gates on a trapped-ion quantum computer, Phys. Rev. Lett. **126**, 220503 (2021).

[55] R. Belyansky, P. Bienias, Y. A. Kharkov, A. V. Gorshkov, and B. Swingle, Minimal model for fast scrambling, Phys. Rev. Lett. **125**, 130601 (2020).

[56] Z. Li, S. Choudhury, and W. V. Liu, Fast scrambling without appealing to holographic duality, Phys. Rev. Res. **2**, 043399 (2020).

[57] C. Yin and A. Lucas, Bound on quantum scrambling with all-to-all interactions, Phys. Rev. A **102**, 022402 (2020).

[58] L. García-Álvarez, I. L. Egusquiza, L. Lamata, A. del Campo, J. Sonner, and E. Solano, Digital quantum simulation of minimal AdS/CFT, Phys. Rev. Lett. **119**, 040501 (2017).

[59] J. Martyn and B. Swingle, Product spectrum ansatz and the simplicity of thermal states, Phys. Rev. A **100**, 032107 (2019).

[60] V. P. Su, Variational preparation of the thermofield double state of the Sachdev-Ye-Kitaev model, Phys. Rev. A **104**, 012427 (2021).

[61] A. R. Brown, H. Gharibyan, S. Leichenauer, H. W. Lin, S. Nezami, G. Salton, L. Susskind, B. Swingle, and M. Walter, Quantum gravity in the lab: Teleportation by size and traversable wormholes (2021), arXiv:1911.06314 [quant-ph].

[62] S. Nezami, H. W. Lin, A. R. Brown, H. Gharibyan, S. Leichenauer, G. Salton, L. Susskind, B. Swingle, and M. Walter, Quantum gravity in the lab: Teleportation by size and traversable wormholes, part II (2021), arXiv:2102.01064 [quant-ph].